Journal of Applied Polymer Science

Investigation of structure and mechanical properties of toughened poly(L-lactide)/thermoplastic poly(ester urethane) blends

Erfan Oliaei, Babak Kaffashi, Saeed Davoodi
School of Chemical Engineering, College of Engineering, University of Tehran, P.O. Box 11365-4563, Tehran, Iran. Tel: + 98 21 66967789, Fax: + 98 21 66957784
Correspondence to: B. Kaffashi (E-mail: kaffashi@ut.ac.ir)

ABSTRACT: In this study, poly(L-lactide) (PLA) is melt-blended with thermoplastic polyurethane (TPU) to modify the brittleness of PLA. An aliphatic ester-based TPU was selected in order to have an ester sensitivity for degradation and an inherent biocompatibility. Using this compatible TPU, there was no need to apply problematic compatibilizers, so the main positive properties of PLA such as biocompatibility and degradability were not challenged. The detected microstructure of PLA/TPU blends showed that when the TPU content was lower than 25 wt %, the structure appeared as sea-islands, but when the TPU content was increased, the morphology was converted to a cocontinuous microstructure. A higher interfacial surface area in the blend with 25 wt % TPU (PLA25) resulted in a higher toughness and abrasion resistance. The various analyses confirmed interactions and successful coupling of two phases and confirmed that melt-blending of PLA with the aliphatic ester-based TPU is a convenient, cost-effective, and efficient method to conquer the brittleness of PLA. The prepared blends are general-purpose plastics, but PLA25 showed an optimum mechanical strength, toughness, and biocompatibility suitable for a wide range of applications. © 2015 Wiley Periodicals, Inc. J. Appl. Polym. Sci. **2016**, *133*, 43104.

KEYWORDS: biopolymers and renewable polymers; compatibilization; morphology; polyurethanes; rheology

Received 10 August 2015; accepted 26 October 2015
DOI: 10.1002/app.43104

INTRODUCTION

Poly(L-lactide) (PLA) is a green, renewable, biodegradable, and environmentally friendly polymer. One disadvantage of this notable polymer is its brittleness, which limits its applications. Another drawback is its low melt strength, due to the lack of viscoelasticity, limiting its applications in packaging and film production. Nowadays, the petrochemical-based polymers are widely used because of their low cost, high-speed production, high mechanical performance, good barrier properties, and good heat stability; however, they have manifested several drawbacks. Some of them are declining oil and gas resources, fluctuating oil and gas prices, concerns for their degradation and environmental issues, accelerating global warming, generation of cross-contamination during recycling, and the toxicity risk of their trace monomers or oligomers in food-contacting products.[1–3] The mentioned drawbacks are negligible for biopolymers, so nowadays most of them are found in many applications.[3,4] PLA is an aliphatic biopolyester that has outstanding advantages not only over commodity polymers but also over many other biopolymers. PLA is biodegradable, biocompatible, and recyclable,[5] and its production consumes 25 to 55% less fossil energy compared with the petroleum-based polymers. It has also several advantages over other biopolymers since their monomers are obtained by fermentation of corn, sugar beets, wheat, and rice. Also, its application improves the agricultural economy and reduces CO_2 emissions in high amounts during their production (in some grades the net emitted CO_2 is negative), which helps to reduce global warming and helps easier and more diverse processing technologies to emerge.[1–3,6–12] Although the tensile strength and elastic modulus of PLA are comparable with the commonly used poly(ethylene terephthalate) and it has many advantages, poor toughness (elongation at break less than 10%) limits its usage in many applications.[2,6,9,13–21]

To obviate the brittleness drawback of PLA, there are several proposed modifications, such as copolymerization, plasticization, and blending with other polymers. However, copolymerization is not an economical method for some applications, and plasticization is a temporary method because of migration of plasticizers in the matrix. Furthermore, most of the mentioned methods lead to the polymer blends with poor mechanical properties and reduced biodegradability and biocompatibility.[6,8,9,22,23]

On the other hand, polyurethanes are a family of polymers with good properties. Some of them show biodegradability, biocompatibility (even compatible with blood), and flexibility.[24] Within this family, the thermoplastic polyurethanes (TPU) are

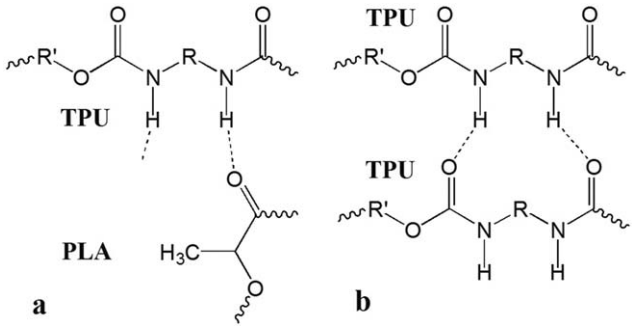

Figure 1. Possible hydrogen bonding in PLA/TPU blends: (a) between PLA and TPU, (b) between TPU chains.

interesting materials that have flexibility, biocompatibility, abrasion resistance, oil and solvent resistance, and biological stability. The biocompatibility of TPU and PLA is approved by the U.S. Food and Drug Administration (FDA), and both are widely used, even for high-risk biomedical applications.[15] The commercially available TPU is a linear segmented block copolymer[25] composed of soft and hard segments; the mechanical properties can be adjusted by the ratio of such segments. Thus, these flexible, biodegradable, and durable polymers are good candidates to improve PLA brittleness.[15,17,22,23,26] Several successfully toughened blends of PLA/TPU proved the toughening ability of TPU for PLA.[8,14,22,25–30]

However, some of these materials are immiscible with PLA and compatibilizers are required, even though it is understood that the existence of these materials limits the biocompatibility of the final products.[26,31] This work aims to assess the toughening ability of TPU in PLA/TPU and its compatibility without the use of compatibilizers.

In the current work, previously synthesized poly(L-lactide) and a TPU with high molecular weight were melt-blended. The ester-based TPU with higher molecular weight was used because of its fine miscibility and interactions with PLA. Furthermore, the melted blends were mixed for a time long enough to allow for more interactions and compatibility; hence the plastic blends were prepared with no compatibilizers. The hydrogen bonding occurred between —NH and —C═O (in PLA, ester and urethane groups of TPU), as clearly shown by the Fourier transform infrared spectroscopy (FTIR) characterizations. At the molecular scale, the PLA chains are miscible with the soft esteric segments of TPU, and this hydrogen bonding fortifies the PLA and TPU interactions (Figure 1).[18]

There are some other ways to generate chemical interactions between the different parts. For instance, the isocyanate groups at the end of the TPU chains can react with the hydroxyl and carboxyl groups at the end of the PLA chains, as shown in Figure 2.

The isocyanate groups at the ends of TPU chains may react with the terminal hydroxyl groups of PLA or TPU chains. The produced urethane groups may then react with isocyanate, leading to a branched product [Figure 3(a)]. In Figure 3(b), first, the carboxyl group of PLA or TPU reacts with the isocyanate and generates unstable *O*-acylcarbamate groups; this group

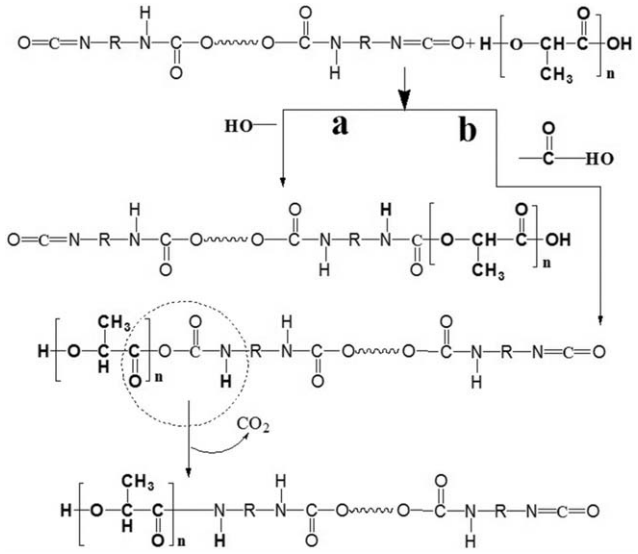

Figure 2. Possible reactions of TPU with (a) hydroxyl-terminated or (b) carboxyl-terminated chains of PLA.

quickly releases CO_2 and is changed to an amide. This amide group can also react with isocyanate, leading to a branched or crosslinked product.[31–34]

The reaction in Figure 3(a) is more likely to proceed, due to the higher rate of reaction between the hydroxyl and isocyanate groups than the reaction rate between carboxyl and isocyanate groups. Moreover, the reaction rate of isocyanate with the hydroxyl group is much higher than the reaction rate of isocyanate with the amide group. Hence, it is more probable that the molecular weight of the PLA matrix is increased by the extension of chains in a linear manner than by creating branches. Furthermore, three types of transesterification may have occurred, which are due to the presence of hydroxyl, carboxyl, and ester groups (Figure 4). The low concentration of end carboxyl groups accelerates the reaction rates. Even though these reactions cannot increase the molecular weight of the chains, they can change different parts, causing more compatibility in the blends.[35]

Moreover, the dynamic rheological analysis showed high melt elasticity and low-frequency crossover. This also confirms chain entanglements and the molecular interactions of PLA with TPU in the blends.[25,31,36,37]

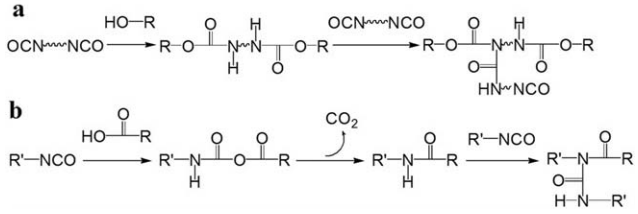

Figure 3. Probable chemical reactions in PLA/TPU blends: (a) reactions of terminal isocyanate groups with —OH terminal groups (R: PLA or TPU); (b) reactions of —NCO with —COOH terminal groups (R: PLA or TPU). (Reproduced from ref. 31 with permission from John Wiley & Sons, Inc.)

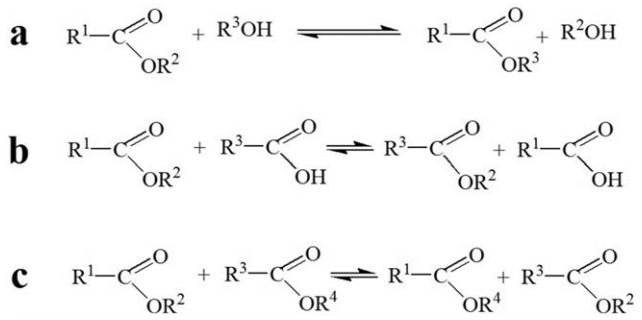

Figure 4. Three types of transesterification reactions: (a) alcoholysis, (b) acidolysis, and (c) ester–ester interchange.

Scanning electron microscopy (SEM) confirmed that in the blends with low TPU content the structure has a sea-island structure, but when the TPU content rises, the structure is converted into a cocontinuous structure. The mechanical properties are directly affected by the structure. For instance, the tensile behavior of the blends was completely changed by conversion of the structure. Finally, based on all of the characterizations, particularly the mechanical characteristics, the optimum bioplastic blend (PLA25) was suggested. Due to its biodegradability, biocompatibility, and high melt elasticity, it has the potential to be applied in many fields, such as electrospinning, medical applications, the production of thermoformed containers, and thermal sealing.

EXPERIMENTAL

Materials

PLA was synthesized from the purified L-lactide prepared by L-lactic acid. The ring-opening polymerization was performed for the dried L-lactide monomers via the reactive extrusion method, as clearly demonstrated in previous works.[38,39] The PLA molecular weight (M_w) and its polydispersity index (PDI) were calculated with three different methods to be a M_w of 120,000 g mol^{-1} and a PDI equal to 1.78.[38] The supplied TPU, thermoplastic poly(ester urethane), was commercially available from the COIM Group, Settimo Milanese, Milan, Italy, with a grade name LPR 9020T. Gel permeation chromatography (GPC) was carried out to delineate the molecular weight and the molecular weight distribution of the purchased TPU using an Agilent GPC 1260 chromatograph, Agilent Technology, Santa Clara, California. The 1 mg mL^{-1} solution of TPU in pure tetrahydrofuran (THF) was characterized via standard swelled polystyrene in a THF column. The method was carried out according to ASTM D 6579. The results exhibited a M_w of 227,140 g mol^{-1} and a PDI equal to 2.69. The thermoplastic polyurethanes are block copolymers that are usually synthesized by the reaction of diisocyanates and oligomeric low-molecular-weight diols (the so-called chain extenders). The oligomeric, high-molecular-weight (600–4000 g mol^{-1}) diols usually consist of soft segments, while their hard segments are composed of diisocyanates and low-molecular-weight (60–400 g mol^{-1}) diols.[16] THF for gel permeation chromatography (LiChrosolv) and highly pure *N*,*N*-dimethylformamide (DMF) for the removal of TPU in morphological studies were used, and both were purchased from Merck Chemicals, Darmstadt, Germany.

Sample Preparation

The PLA and TPU granules were vacuum-dried at 80°C for 4 h. They were then melt-blended with an internal mixer (Brabender 50 EHT, Duisburg, Germany, with a rotational speed of 60 rpm for 15 min).[40] The PLA and TPU were simultaneously loaded into a mixing chamber in several compositions. They were coded as PLA followed by a number representing the weight percent of TPU in the blend. For instance, PLA5 contains 5 wt % TPU and 95 wt % PLA. The stock temperature in the mixer was 190°C. The final blends were hot-pressed at 190°C to form different specimens for all measurements and then were cooled to room temperature.[13,26]

Scanning Electron Microscopy (SEM)

The morphology of the samples was observed with an AIS2100 scanning electron microscope (Seron Technology, Uiwang, South Korea) with an accelerating voltage of 12 kV. The samples were cryogenically fractured after 10 min immersion in liquid nitrogen. Some of them were treated by DMF in order to remove the TPU phase.[15] All of the sample surfaces were treated and sputter-coated with gold before being studied by the SEM.

Mechanical Testing (Tensile, Impact, Hardness, and Abrasion)

Tensile Test. The tensile measurements of the PLA/TPU blends were performed by a Gotech universal AI-7000-LA material testing machine (Taichung, Taiwan) according to ASTM D638. The specimens were dumbbell-shaped with a thickness of 4 mm. Their overall and narrow section widths were 6 and 19 mm, respectively. Also, the overall and narrow section lengths of the dumbbell-shaped specimens were 33 and 115 mm. The specimens were held tightly between the static and moving clamps at room temperature. The upper clamp was raised at a rate of 5 mm min^{-1} until the specimens broke. At least three specimens were tested to get an average value for each sample.

Impact Measurements. The edgewise unnotched Charpy test was performed for all samples according to ISO 179/3 e U. The impact properties of the samples were measured by a Frank Baldwin Model BLI pendulum impact testing machine, Frank Bacon Machinery Sales Company, Michigan. At least three specimens of each sample were tested.

Hardness Test. The sample hardness was measured by a Shore D durometer (Frank testing machine, Frank Bacon Machinery Sales Company, Warren, Michigan). For each sample, at least three specimens were tested at different points according to DIN 53505.

Abrasion Resistance. The abrasion was tested with the Frank abrasion tester (rotary drum abrader, Model-Karl Frank, Munich, Germany). At least three specimens of each sample were tested to get an average value. The method was carried out according to ASTM D 5963 (method A) with a drum diameter of 150.0 mm and a rotation speed of 40 ±1 rpm. Furthermore, the loaded force and drum length were 9.807 N and 500 mm, respectively.

The abrasion resistance index (ARI) can be calculated using eq. (1):

$$\mathrm{ARI}=\frac{\Delta m_s \times d_t}{\Delta m_t \times d_s}\times 100 \qquad (1)$$

where Δm_s is the mass loss of the standard rubber/thermoplastic elastomer after an abrasion distance of 40 m; Δm_t is the mass loss

of the test sample in the stated distance; d_t is the density of the test sample; and d_s is the density of the standard rubber or thermoplastic elastomer.[41] The standard sample for ARI measurements of elastomers is recommended to be natural rubber, particularly the Standard Malaysian Rubber 5 (SMR 5) with certain amounts of additives. In this work, it is more logical to consider the pure TPU as the standard because of having both thermoplastic and elastomeric properties along with high abrasion resistance, and above all, being comparable with its derivative blends.

The volume loss is calculated by the conversion of the measured mass losses based on the available standard.

Dynamic Mechanical Thermal Analysis

The dynamic mechanical thermal analysis (DMTA) was performed using an EXSTAR SII DMS6100 (Chiba, Japan) in the tensile mode over temperatures ranging from −75 to 120°C. The heating rate was fixed at 3°C min^{-1}. Several measurements for each sample were carried out at various frequencies.

The shift factor represents the characteristics of the relaxation processes of specific polymers. The shift factor of the master curve is determined by the Williams-Landel-Ferry (WLF) equation using the EXSTAR SII DMS6100 software:

$$\log a_T = \frac{-C_1(T-T_0)}{C_2+(T-T_0)} \quad (2)$$

where T_0 is the reference temperature and usually is selected as a temperature near T_g, and C_1 and C_2 are empirical constants depending on the reference temperature. This time–temperature superposition underlies the construction of the master curve by shifting the points as below[42]:

$$E'(a_T\omega, T) = E'(\omega, T_0) \quad (3)$$

$$E''(a_T\omega, T) = E''(\omega, T_0) \quad (4)$$

Differential Scanning Calorimetry

The thermal behavior of PLA, TPU, and PLA/TPU blends were evaluated using a differential scanning calorimetry (DSC) analyzer (Mettler Toledo DSC 1 Star System, PetalingJaya, Malaysia). The DSC measurements were performed at a heating rate of 10°C min^{-1} under nitrogen atmosphere. At first, the samples were heated from 25 to 120°C to remove any previous thermal histories, then cooled and reheated. The second thermal scanning of samples is reported from −60 to 260°C.

The degree of crystallinity (X_c) of the samples was evaluated by the most commonly used eq. (5)[7,13,16,17]:

$$X_c = \frac{\Delta H_m - \Delta H_c}{w_f \Delta H_m^0} \times 100\% \quad (5)$$

where ΔH_m and ΔH_c are the enthalpies of melting and cold crystallization, respectively, and w_f and ΔH_m^0 are the weight fraction of poly(L-lactide) and heat of fusion of 100% crystalline poly(L-lactide), respectively.

Water Contact Angle Measurements

The contact angle (CA) of deionized water (surface tension: 73.2 mNm^{-1}) was measured by dropping a droplet of 5 μL at ambient temperature. A Kruss G10 apparatus (Hamburg, Germany) was implemented for these measurements. The distance of the vibrating syringe was about 5 cm, and all contact angles were obtained at the initial stage (i.e., < 10 s). Every CA was measured at three or four different points of the surface for individual samples. Each water droplet also has a right and left CA, so at least six different contact angles were used to calculate the average CA for each sample. The deviation of every CA measured in this study was less than 1.5°.

Dynamic Rheological Analysis

The rheological properties were characterized using an Anton Paar Physica MCR 102 (Graz, Austria) with parallel-plate geometry (diameter of 25 mm). All of the rheological measurements were accomplished at 190°C, under air, and based on ASTM D 4440. A gap of 0.5 mm was selected to limit the contact area of molten polymer with air to neglect the possibility of thermo-oxidative degradation.[38] To set a suitable strain for frequency and time sweep runs and to ensure that the applied strain did not exceed the limit of linear viscoelasticity, the strain sweep (from 0.01 to 100%) was initially performed for each sample at a fixed frequency of 10 $rads^{-1}$. The strain amplitudes less than 2.5% ensured a linear viscoelastic response for all samples. The frequency sweep was performed at the strain amplitude of 1% and frequency range of 0.05–500 $rads^{-1}$. The time sweep was performed at the strain amplitude of 1% and angular frequency of 10 $rads^{-1}$.

Attenuated Total Reflection Fourier Transform Infrared Spectroscopy

The infrared spectroscopy of the samples was performed using the attenuated total reflection (ATR) technique by a Bruker Tensor 27 spectrometer (Billerica, Massachusetts) in the frequency range of 600–4000 cm^{-1}.

RESULTS AND DISCUSSION

Phase Morphology

The morphology of both the untreated and DMF-treated surfaces of the samples were analyzed and presented. The DMF partially dissolves the TPU phase on the surface to help in the detection of the blend morphologies.[15] The comparisons of DMF-treated and untreated surfaces (Figure 5) are beneficial for understanding the real morphology of the blends. As can be seen, in PLA10 the TPU spheres are distributed in the PLA matrix, showing a globular structure or island morphology. By analyzing Figure 5, it is obvious that the TPU spherical particles are distributed in the PLA part of PLA25, but the SEM observation of PLA25 treated by DMF shows that the TPU particles are joining together, leading to the cocontinuous morphology. As is shown in Figure 5, PLA40 illustrates a continuous morphology for both PLA and TPU. A good distribution of TPU in the PLA matrix has a direct influence on the improvement of mechanical properties.[34] The two scale SEM observations of untreated fractured blend surfaces provide a good overview of the phases. By analyzing Figure 5(a) and (b), the number of pulled-out TPU particles are negligible, meaning high compatibility of PLA and TPU due to high interfacial interactions.[16]

Altogether, it can be concluded that blends containing low TPU content have a porous structure, but when the TPU content reached about 25 wt %, there is a hybrid of porous and

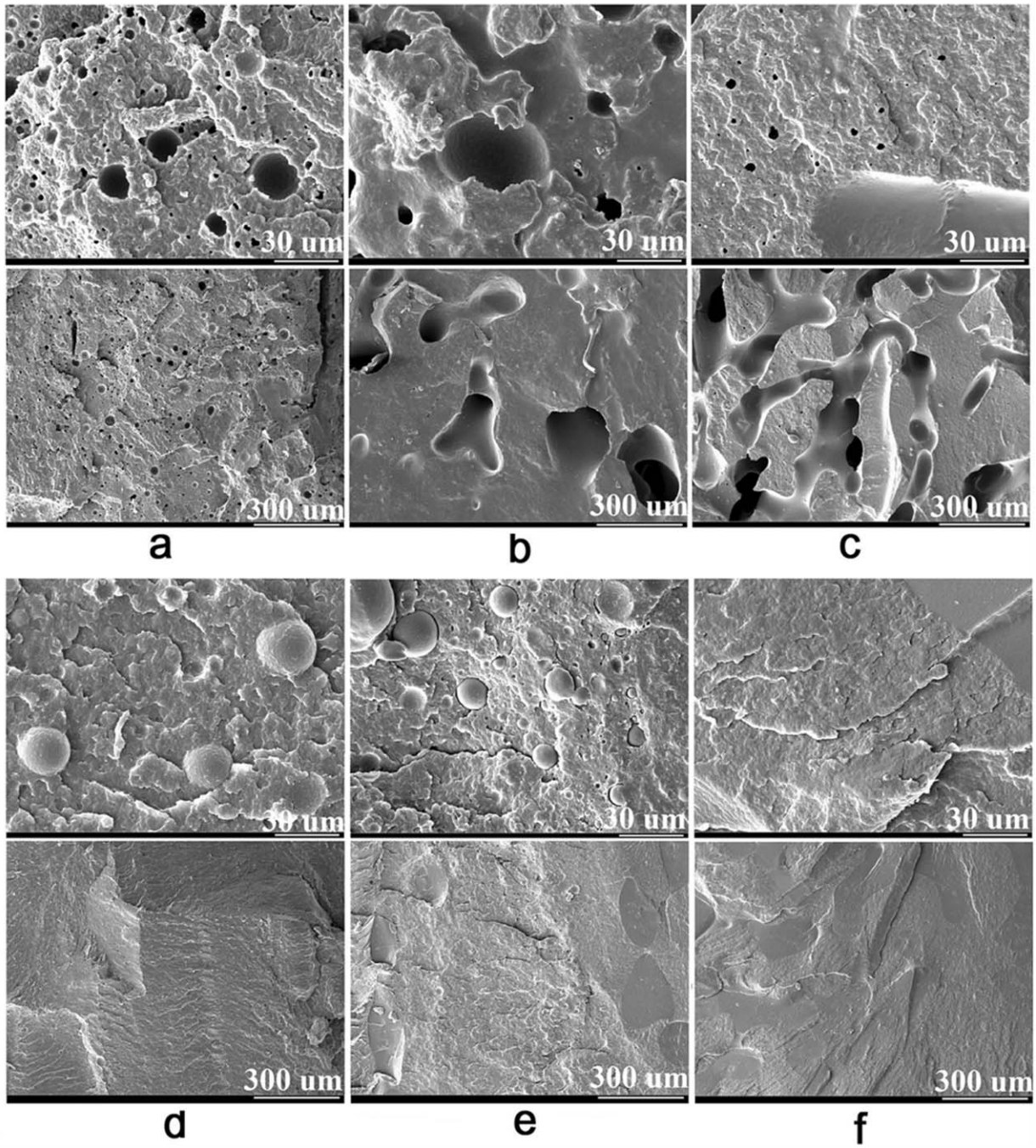

Figure 5. SEM micrographs of cryogenically fractured surfaces of (a) PLA10, (b) PLA25, and (c) PLA40 treated with DMF to partially remove TPU, and untreated cryogenically fractured surfaces of (d) PLA10, (e) PLA25, and (f) PLA40.

spongy structures after TPU removal (the cocontinuous morphology). Further increasing the TPU content in the blend up to 40 wt %, a cocontinuous morphology is observed. Based on the changes in morphologies, the variation in tensile behavior of these blends in the stress–strain curves is justified. The small amount of TPU in the blends causes a normal rupture of the test sample, but for amounts of TPU more than 25 wt %, an obvious necking in the tensile behavior has occurred.

Mechanical Properties

The stress–strain curves of the PLA/TPU blends are illustrated in Figure 6. This figure shows that the neat PLA has a brittle rupture with a low elongation at break at about 2.71%, even though it shows a high tensile strength of about 66.22 MPa. Such results have confirmed the brittle and rigid structure of neat PLA. The addition of TPU in small amounts not only reduced its elongation at break but also decreased its tensile strength. As shown in Figure 6, the increase in TPU from 5 to

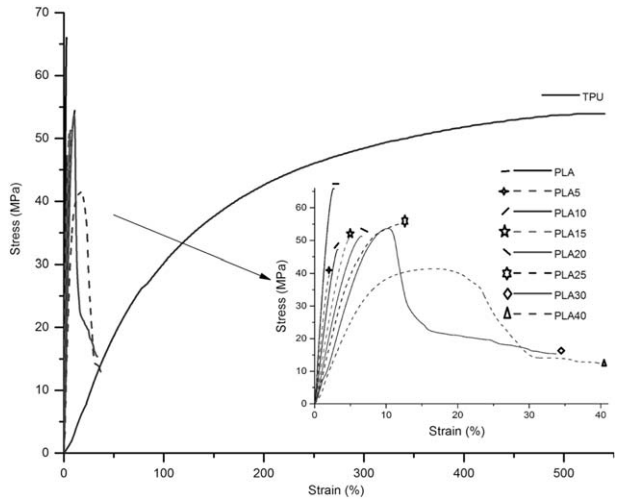

Figure 6. Stress–strain curves of pure and blend samples; first part of curves enlarged to give a clearer view.

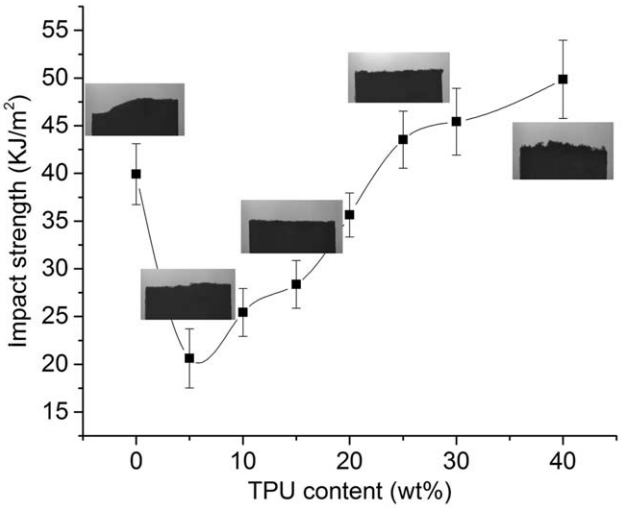

Figure 7. Edgewise unnotched Charpy impact strength of the samples with various TPU contents.

25 wt % results in a large tensile strength. The samples PLA, PLA5, PLA10, PLA15, PLA20, and PLA25 have distinct yield points due to an immediate failure, which is an indication of PLA domination in the matrix of these blends.

The samples PLA30 and PLA40 have different stress–strain behavior with clear yield points (of 53.6 and 41.8 MPa, respectively) following the deformation up to rupture (having elongations of 33.7 and 40.1%, respectively). The elastic stress plateau after stress whitening and the larger elongation at break may be an indication of TPU phase domination in these blends.

As is demonstrated in Table I, the toughness values of PLA5 and PLA10 are less than that of PLA, but for the other blends higher toughness and elongation at break are observed. These elongation and toughness values were raised with increasing TPU content in the blend. PLA25 is considered to be the most appropriate sample with an optimum modulus of 1 GPa and an improved toughness (about four times greater than that of pure PLA).

Based on the data obtained and represented in Figure 7, the Charpy impact strength shows different behavior for different samples. Increasing the TPU content up to 20 wt % in the PLA matrix decreases the Charpy impact strength compared with the neat PLA, but increasing the TPU in the PLA matrix raises the Charpy impact strength. The fractured surfaces of PLA25, PLA30, and PLA40 after impact testing and the ruptured surfaces of these samples after tensile measurements show the existence of some microfibers. These microfibers are not so apparent in other samples, most notably for PLA5. This fibrous structure dissipates the energy and enhances the toughness of these samples.[28,43] Actually, the enhanced impact strength is considered to be the reason for the toughness improvement.[29]

In Table I, it is obvious that the hardness of samples decreases with increasing TPU concentration in the blend. This can be attributed to the good dispersion of TPU in the matrix that inherently contains soft segments, causing a lack of hardness in the blends.[43]

Abrasion Resistance

The abrasion or the volume loss of the samples is depicted in Figure 8, and the abrasion resistance indices are listed in

Table I. Mechanical Properties: Tensile, Hardness, and Abrasion Properties of Samples

Samples	Tensile strength (MPa)	Yield strength (MPa)	Elastic modulus (GPa)	Elongation at break (%)	Toughness (MJ/m^3)	Hardness (Shore D)	ARI (%)
PLA	66.22±4.22	—	3.77±0.04	2.71±0.13	1.07±0.08	74±3	20.4±3.0
PLA5	39.45±3.45	—	2.58±0.08	2.10±0.10	0.47±0.04	71±4	24.2±2.5
PLA10	47.22±3.67	—	1.99±0.08	3.28±0.22	0.86±0.10	69±2	31.4±2.1
PLA15	50.73±3.01	—	1.41±0.11	4.80±0.19	14.88±0.09	68±4	26.9±1.8
PLA20	51.21±2.78	—	1.16±0.07	6.62±0.21	2.01±0.11	66±4	34.6±2.1
PLA25	55.01±2.65	—	0.98±0.09	12.12±0.12	4.60±0.06	64±3	61.8±2.0
PLA30	15.32±1.23	53.68±4.13	0.85±0.03	33.77±0.70	8.64±0.11	63±2	45.3±2.4
PLA40	12.37±2.34	41.88±2.91	0.58±0.12	40.16±0.89	10.52±0.10	61±4	42.6±1.1
TPU	53.92±2.67	—	0.58±0.07	541.20±20.43	224.97±10.83	45±1	100±0.5

ARI of PLA, TPU, and PLA/TPU blends calculated by assuming ARI of the TPU as 100%.

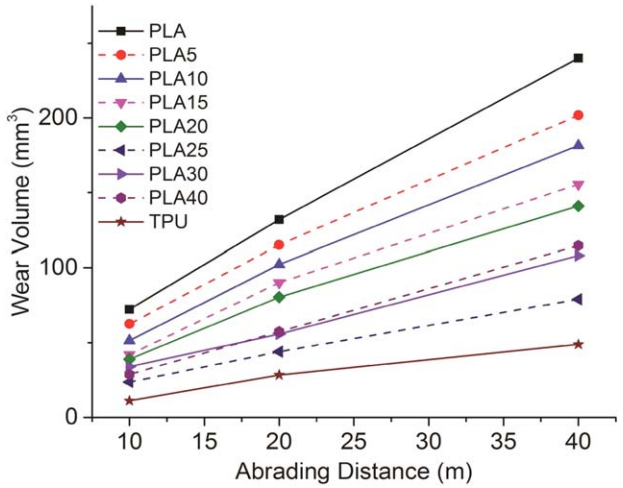

Figure 8. Wear volume of different PLA/TPU blends and TPU as function of abrading distance. [Color figure can be viewed in the online issue, which is available at wileyonlinelibrary.com.]

Table I. As is shown, the abrasion resistance is increased by the presence of more TPU in the blend, but in an irregular manner. The results indicate that PLA25 had the largest ARI among all the blends, even larger than the ARI of PLA30 and PLA40. For PLA25 this may result in better dispersion of TPU and optimum interactions between PLA and TPU. It can be clearly seen that the ARI values of blends with 30 and 40 wt % TPU are almost constant. Also, it is evident that the trend of the wear volume loss is almost a linear function of abrading distance.[44]

Thermal Properties

The DMTA was implemented to investigate the miscibility and phase interaction of PLA/TPU blends for different TPU concentrations. Figure 9 displays the storage and loss moduli of the blends as a function of temperature. The storage moduli of the blends are decreased with increasing temperature. Also, the storage modulus at temperatures higher than 0°C is reduced with increasing TPU. The loss modulus (E'') and loss factor (tan δ) may be used interchangeably to measure the characteristic temperatures pertaining to various relaxation processes, even

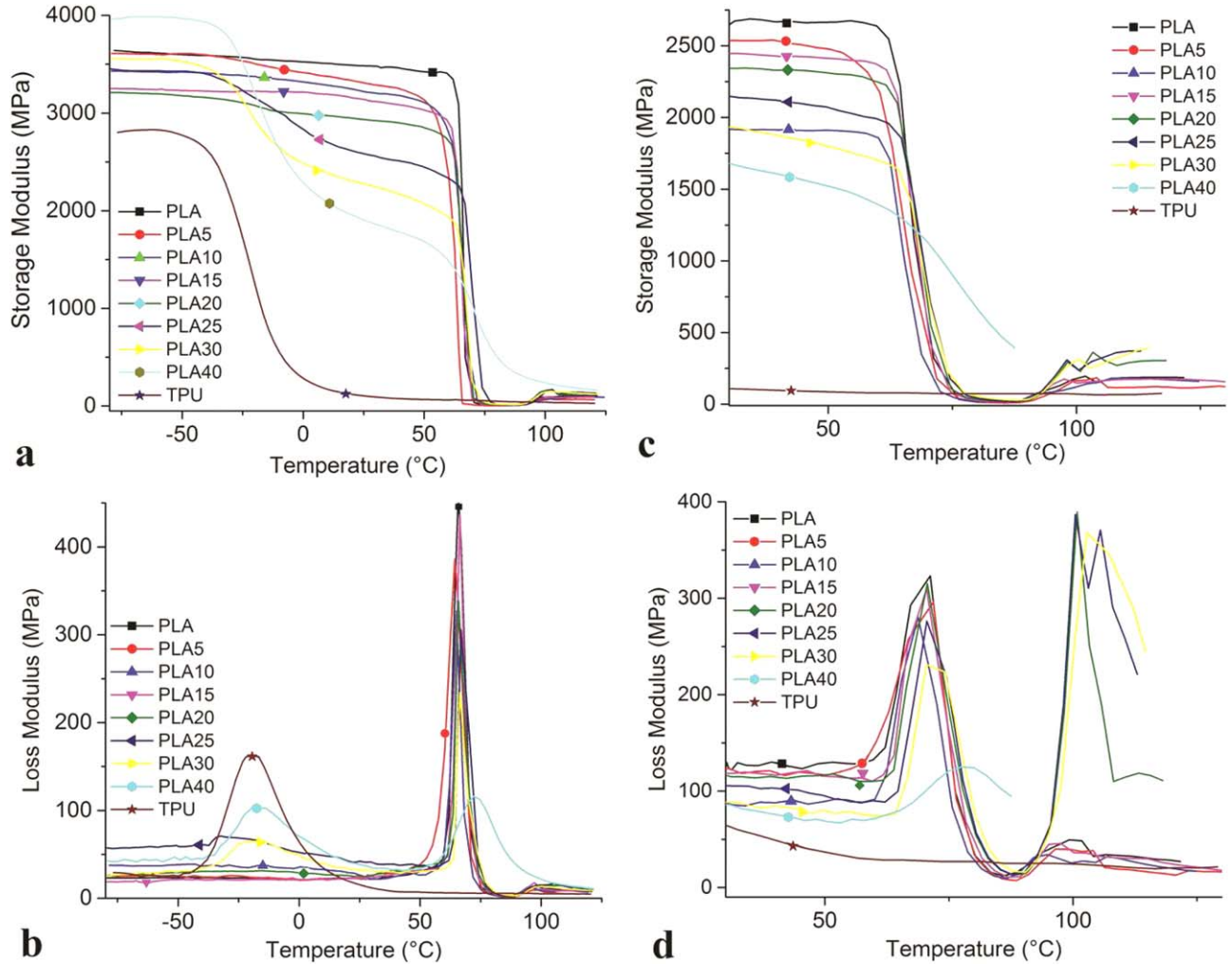

Figure 9. (a) Storage and (b) loss moduli of samples with different PLA/TPU ratios at frequency of 5 Hz; (c) storage and (d) loss moduli of samples with different PLA/TPU ratios at frequency of 100 Hz. [Color figure can be viewed in the online issue, which is available at wileyonlinelibrary.com.]

Table II. Thermal Properties of Samples

Samples	$T_{g,TPU}$[a] (°C)	$T_{g,PLA}$[a] (°C)	$T_{g,TPU}$[b] (°C)	$T_{g,PLA}$[b] (°C)	$T_{m,TPU}$ (°C)	T_c (°C)	$T_{m,PLA}$ (°C)	$\Delta H_{m,PLA}$ (J g^{-1})	$X_{t,PLA}$[c] (%)
PLA	—	65.71	—	55.57	—	136.05	168.89	39.35	42.31
PLA5	—	64.31	—	53.87	—	125.25	169.77	39.00	44.14
PLA10	−16.46	64.99	N M	N M	N M	N M	N M	N M	N M
PLA15	—	66.37	—	53.92	—	124.86	167.98	35.29	44.64
PLA20	−14.82	65.84	N M	N M	N M	N M	N M	N M	N M
PLA25	−23.81	66.91	—	54.43	—	123.88	168.57	31.11	44.60
PLA30	−15.56	66.44	—	53.39	204.19	123.79	169.47	29.09	44.69
PLA40	−15.81	72.13	—	57.94	203.39	123.91	168.66	24.98	44.77
TPU	−18.57	—	−26.71	—	183.17	—	—	—	—

N M = not measured.
[a] Obtained by DMTA measurements via $f = 5$ Hz.
[b] Obtained by DSC measurements.
[c] Considering the melting enthalpy of 100% crystalline poly(L-lactide) 93 J g^{-1}.

though there are small differences between the characteristic temperatures of E'' and tan δ.[29] In Figure 9, the loss modulus of PLA shows a peak at 65.7°C, and the loss modulus of TPU shows a peak at −18.5°C. These peaks show that their glass-transition temperatures rise due to the chain segment motions.[25] The DMTA plots of E'' show two apparent peaks for some of the blends, indicating the presence of two different continuous phases in the blends at a microscopic level. Actually, these two peaks are attributed to the T_g of the PLA-rich and TPU-rich phases. This demonstrates that in such cases PLA and TPU are not completely miscible.[25,26,29] The first peak (about −18°C) is not clearly shown for the blends having TPU content less than 25%, but the second peak (∼65°C) is obvious for PLA and all the other blends, although its height is continuously decreased with increasing TPU. The pure PLA displays a high storage modulus (E') at about 3.5 GPa, which remains in the same order up to 65°C, followed by an abrupt drop to about 50 MPa at 80°C, while pure TPU shows a smoother drop in E' at about −19°C (T_g). For PLA25, PLA30, and PLA40, E' dropped smoothly from −50°C to 20°C, similar to TPU, and again dropped at about 65°C. Although in the systems with TPU less than 25% (with PLA as the continuous phase) E' remains large at temperatures up to 65°C followed by an abrupt drop, there is only one T_g that specifies the presence of a PLA-rich phase.[15] These results are in agreement with the SEM observations of PLA and TPU dispersions in the PLA/TPU blends.

For the majority of formulations, E' drops at about 60–70°C; when the fraction of TPU becomes 30% or higher, a drop appears at lower temperatures that is due to the T_g of TPU. The storage modulus rises again at ca. 100°C, due to the PLA cold crystallization.[26] This is the temperature at which E' starts to increase because of the crystallization of PLA.[17] This transition is shifted to lower temperatures by increasing TPU. The height of the PLA crystallization peak rises with an increase in frequency. At still higher frequencies, E' drops more abruptly at temperatures between 60 and 70°C.[42] As shown in Figure 9, particularly in parts (c) and (d), the height of the crystallization peaks for the samples PLA15, PLA20, PLA25, PLA30, and PLA40 are even higher than the peak height of T_g for the PLA-rich phase at 100 Hz. These results suggest that TPU improves the cold crystallization ability of the PLA in the blends, especially for the high-TPU blends. This is due to the higher mobility associated with the continuous TPU phase structure causing high mobility of PLA chains.[15,17,26] All numerical data of DMTA at different frequencies are summarized in Tables (II and III), and IV.

The time–temperature superposition (i.e., frequency–temperature superposition) theory is applied for PLA25 with the

Table III. T_g of PLA/TPU Blends in PLA-Rich Phase Obtained by DMTA at Different Frequencies

Frequency	PLA (°C)	PLA5 (°C)	PLA10 (°C)	PLA15 (°C)	PLA20 (°C)	PLA25 (°C)	PLA30 (°C)	PLA40 (°C)
10	66.61	65.23	64.52	66.04	65.55	69.44	69.44	74.32
15	66.29	64.71	64.07	65.61	68.90	69.12	69.10	73.98
20	65.98	64.17	66.87	68.32	68.37	68.45	68.45	76.22
30	68.20	68.94	66.59	68.03	67.61	68.13	71.55	75.90
50	67.88	68.38	66.31	67.74	67.32	71.14	71.26	75.59
67	67.57	67.90	65.87	66.95	70.91	70.85	70.79	77.85
100	71.25	71.88	68.79	70.51	70.62	70.54	70.48	77.53

Table IV. T_g of PLA/TPU blends in TPU-Rich Phase Obtained by DMTA at several frequencies.

Frequency	PLA25 (°C)	PLA30 (°C)	PLA40 (°C)	TPU (°C)
10	−30.82	−18.20	−16.13	−18.86
15	−25.34	−18.50	−11.62	−17.01
20	−31.66	−18.77	−14.37	−15.15
30	−23.44	−14.45	−12.22	−15.41
50	−35.80	−19.33	−10.10	−13.50
67	−32.88	−17.31	−12.83	−13.77
100	—	—	−17.92	−14.05

temperature sweep analyses for eight frequencies listed in Tables (II and III), and IV. From these data, a master curve is constructed by horizontal shifting using the built-in EXSTAR SII DMS6100 software. The T_0, C_1, and C_2 of the WLF equation were selected to be 69.4°C (near the T_g of PLA25) and are calculated to be 22 and 16, respectively. The fitted master curve for PLA25 is represented in Figure 10.

Figure 11 shows the DSC heating curves of PLA, TPU, and some PLA/TPU blends. As is easily seen, for the samples except TPU there are three transitions upon heating: the PLA glass transition, the PLA cold crystallization, and a melt peak. The T_g values obtained from the DSC are about 12°C lower than those obtained from DMTA even though the trend is similar. These differences are due to the different measuring mechanisms of DMTA and DSC.[26] As is shown, TPU has a double melting point at about 180–195°C but with a sharper peak at 183.1°C. The enthalpy of fusion of PLA (ΔH_m) in the blends with higher TPU content becomes lower since the PLA concentration is increased.[11,23] The cold crystallization of PLA has some broad peaks at specific temperatures as the incorporation of TPU markedly lowers their occurrence temperatures, suggesting an enhanced crystallization ability of the PLA. Also, a slight decrease in T_g of the PLA-rich phase with small TPU pertains to more flexibility of PLA chains in the blend. This contributes to an increase in the crystallization rate of PLA chains.[25,26] To calculate the degree of crystallinity for the samples, eq. (5) is used, considering that the melting enthalpy of completely crystalline poly(L-lactide) is 93 J g^{-1}.[13,20,38,45] The results show that the degree of crystallinity for the blends is greater than that for the pure PLA, confirming the enhanced crystallization ability of the PLA in the blends.[15] In fact, in these blends, the number of nuclei and the spherulitic growth rate of PLA are possibly increased by adding more TPU, inducing an increase in the crystallization rate.[14] These results can be attributed to the molecular interactions of PLA and TPU.

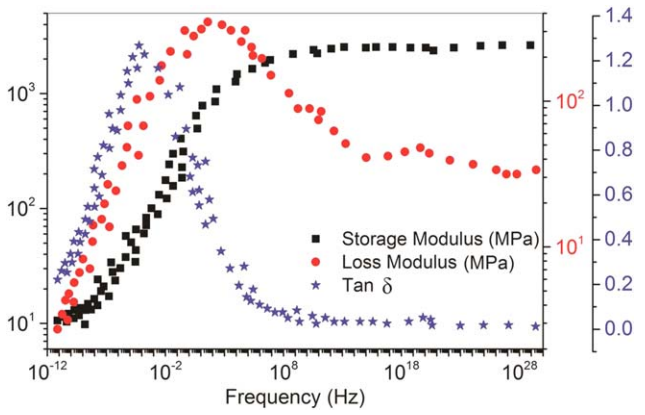

Figure 10. Master curves of PLA25 G' (squares), G'' (circles), and tan δ (stars) drawn by EXSTAR SII DMS6100 software. [Color figure can be viewed in the online issue, which is available at wileyonlinelibrary.com.]

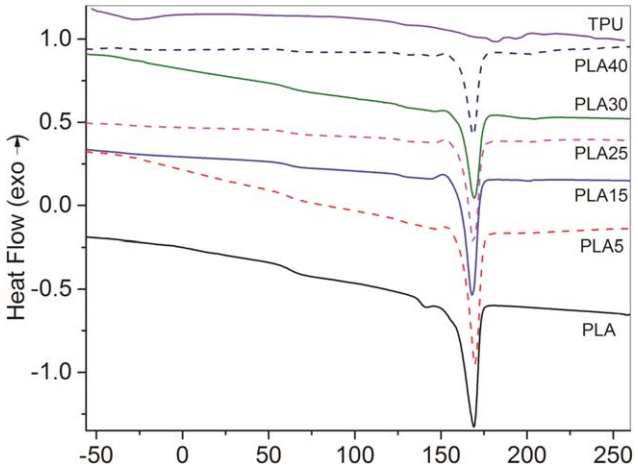

Figure 11. Second DSC heating curves of PLA, TPU, and PLA/TPU blends. [Color figure can be viewed in the online issue, which is available at wileyonlinelibrary.com.]

Water Contact Angle Results

As depicted in Figure 12, the water contact angle of the blends is roughly increased by adding TPU. However, a high TPU concentration results in more hydrophobicity compared to the pure PLA. This is initiated from the structure of two polymers because TPU has less concentration of hydrophilic groups (urethane group), due to the more repeated not-hydrophilic —CH_2— parts in the initial diisocyanates and diols constructing most of the TPU backbone. As a result, TPU shows a higher

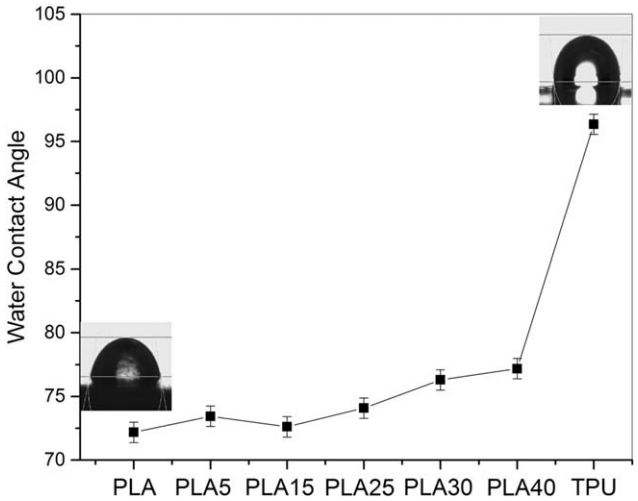

Figure 12. Water contact angle of the samples with various amounts of TPU.

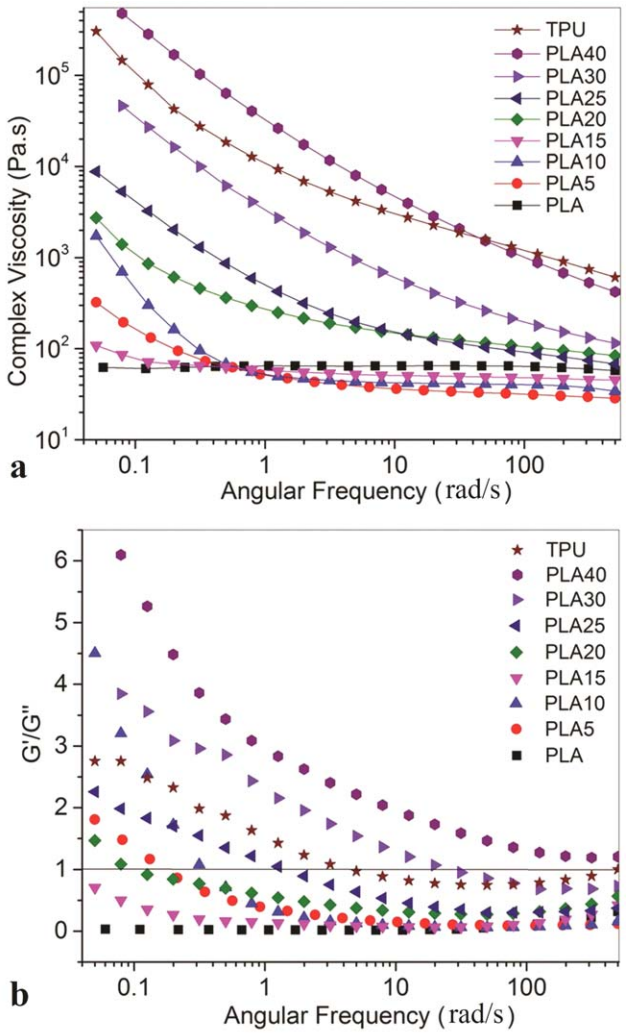

Figure 13. Dependence of (a) complex viscosity and (b) G'/G'' of samples with various TPU contents on frequency; the latter depicts the ratio of elastic to viscous response at different frequencies. [Color figure can be viewed in the online issue, which is available at wileyonlinelibrary.com.]

water contact angle compared with that of PLA, making the blends slightly more hydrophobic.

Rheological Properties

As shown in Figure 13(a), the complex viscosity of blends is increased and shows more shear thinning behavior as TPU contributes to larger viscosity and higher shear thinning (elasticity) of the blend compared to the pure PLA. PLA shows a completely viscous behavior, but this behavior is converted into viscoelastic once blended with TPU. It is obvious that the small fractions of TPU in the blends (PLA5, PLA10, and PLA15) results in less thickening and lower viscosities at low frequencies. It is possible to consider high interactions of small TPU spherical particles in the matrix due to its hard and polar segments, as well as the strong interfacial interactions of TPU and PLA proved by the SEM. The TPU particle interconnectivity and TPU/PLA strong interactions even at low TPU content may behave like a complex network, resulting in a viscosity upturn at low frequencies.[46] This slow response is gradually changed because of the change in morphology.[25,27] Based on the Paul-Barlow theory, the phase inversion for a binary blend is consistently associated with the volume fraction and viscosity ratio of the two phases.[47] As shown for the TPU concentration of about 25 wt %, the blend morphology changes from sea-island to cocontinuous. It is reported that the ratio of storage modulus (G') to loss modulus (G'') can be used to estimate the onset of the morphology transition. As shown in Figure 13(b), the incorporation of TPU into the blend raises the G'/G'' ratio. The enhanced elasticity may stabilize the elongated droplets of the minor phase during melt-blending.[47] The increase in elasticity by the addition of more TPU is not monotonous; PLA30 and PLA40 have more elasticity compared to the pure TPU, due to the high interactions of two polymers (e.g., strong hydrogen bonding, chain entanglements, and possible reacted structures).[25] A very large G'/G'' may be observed at low frequencies for the blends of low TPU content such as PLA5 and PLA10. The reason for such behavior may be related to the dispersed TPU spheres in the matrix acting as rigid fillers.[27]

Figure 14 depicts the G' and G'' of samples as a function of frequency. As is depicted, for PLA a viscous behavior is manifested as G'' dominates G' for the whole frequency range. In the case of TPU, the viscoelastic behavior is different because G' dominates G'' at low frequencies, and after a crossover frequency a viscous behavior is observed. The PLA40 with a higher content of TPU has G' dominating over G'' for entire frequencies, showing the highest relaxation time and an elastic behavior. PLA30 also presents a higher elasticity and longer range for $G' > G''$ compared with those for PLA25. For the PLA/TPU blends and pure TPU, the G'/G'' crossover point is seen at low frequencies, which indicates that chains require a longer time to relax.[48,49] Also, the low angular frequency of the G'/G'' intersection confirms the compatibility of the blends. The addition of TPU to the blend furthers increases the frequency at which G'' becomes greater than G', so it increases the relaxation time and the elastic response. In fact, the addition of TPU increases the time for relaxation of the main chains and branches; in other words, with the rise of TPU content in the blends the speed of relaxation is decreased. As may be seen in Figure 13(b), the PLA/TPU blends show a more elastic response than viscous at low frequencies ($G'/G'' > 1$).[31] The reason may pertain to the increase of chain lengths and branches leading to the physical and chemical interactions of PLA and TPU through molecular entanglements, hydrogen bonding, and so on.

Figure 15 shows the result of time sweeps for PLA, PLA20, and PLA40 as some representatives. As is obvious, the G' and G'' of the PLA fell with time due to the cleavage of chains. For PLA20, G' was higher than G'' and was not significantly changed with time. In the case of PLA40, similar to PLA20, G' is greater than G'' but both moduli are increased with time. Perhaps in the case of PLA40 this behavior relates to the molecular interactions and entanglements preventing the relaxation of PLA and TPU chains.[36] Analyzing Figure 15, the degradation of pure PLA starts after 4 min in the time sweep, and it is an unavoidable drawback of PLA. Although the test results of PLA are obtained from the PLA sample not put into the internal mixer, a batch of internal-mixed PLA was analyzed by GPC, and the results showed that the molecular weight of PLA was not reduced significantly (Figure 16).

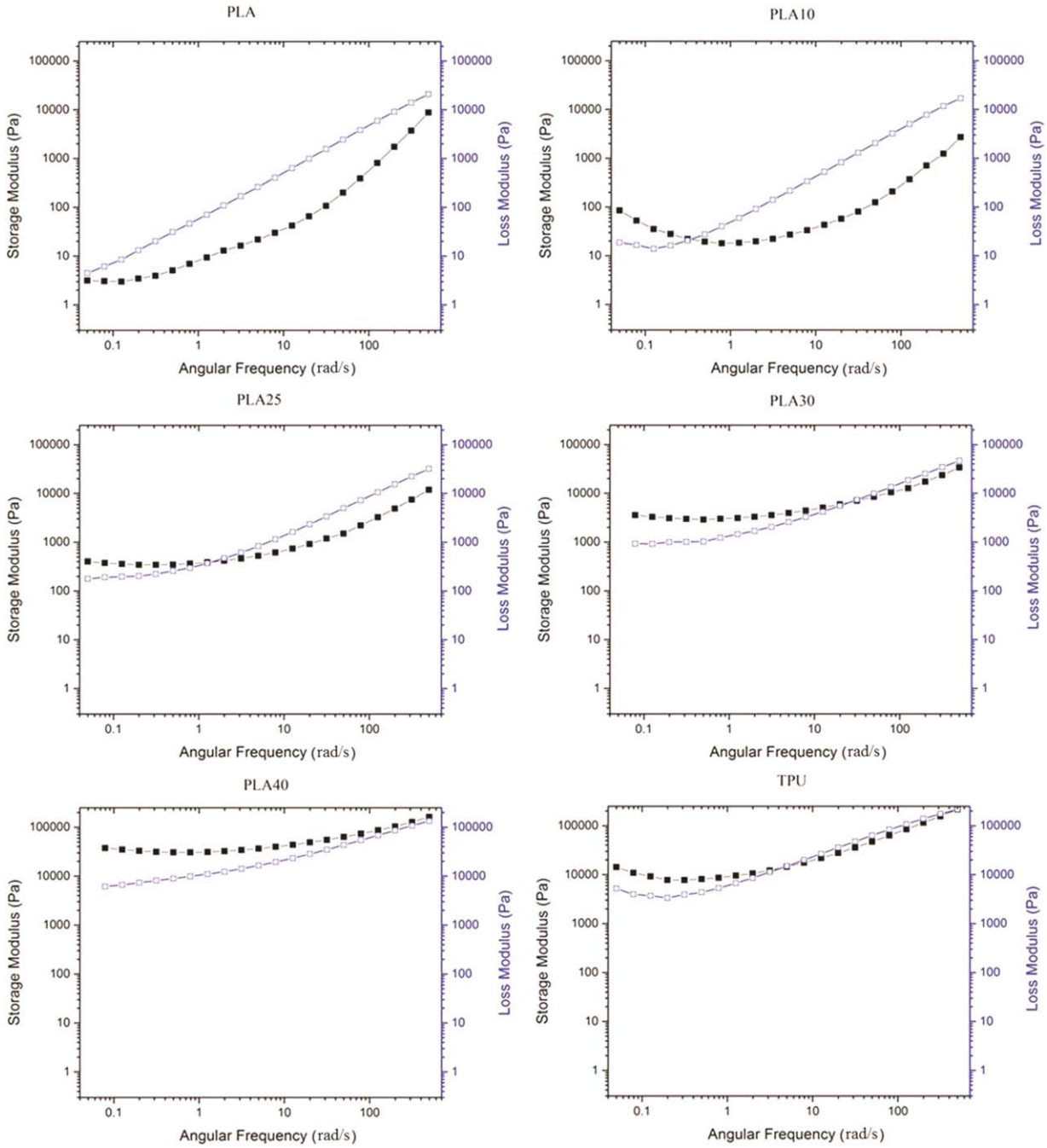

Figure 14. Dependence of storage (filled squares) and loss moduli (open squares) on frequency for PLA, PLA10, PLA25, PLA30, PLA40, and TPU. [Color figure can be viewed in the online issue, which is available at wileyonlinelibrary.com.]

ATR-FTIR Investigation

The FTIR spectra of the PLA/TPU blends are shown in Figure 17. They show several small absorption peaks at ~3450 cm^{-1} corresponding to stretching bands of —NH and —OH in the TPU or PLA structures. In TPU, there are specific absorption peaks at 3323.2 and 1540 cm^{-1} pertaining to the stretching and bending vibrations of —NH groups, respectively.[16,17,27,50] The peak at ~1081 cm^{-1} belongs to the stretching of —C—O— bonds,[16] and the peak at ~1360 cm^{-1} represents the bending of —CH_3 groups in PLA and so cannot be seen for TPU.

The —C—N— bond in TPU has distinctive IR bands at ~1220 and ~1530 cm^{-1}.[16] The —C—C— stretching vibration peaks can be seen at ~870 cm^{-1}.[7] The —CH— vibrations have a multiplicity of weak bands at ~3000 cm^{-1}.[16,38] The —CH— stretching vibrations at ~2995 and ~2920 cm^{-1} (asymmetric and symmetric, respectively) and its bending vibrations at ~1450 cm^{-1} are shown in the PLA spectrum. Furthermore, CH_2 asymmetric and symmetric vibrations at ~2940 and ~2850 cm^{-1} and some distinct peaks at ~1529, 1587, and 3321 cm^{-1}, which show C═C—, —C—N—, and —NH groups, respectively, are seen for TPU.[27]

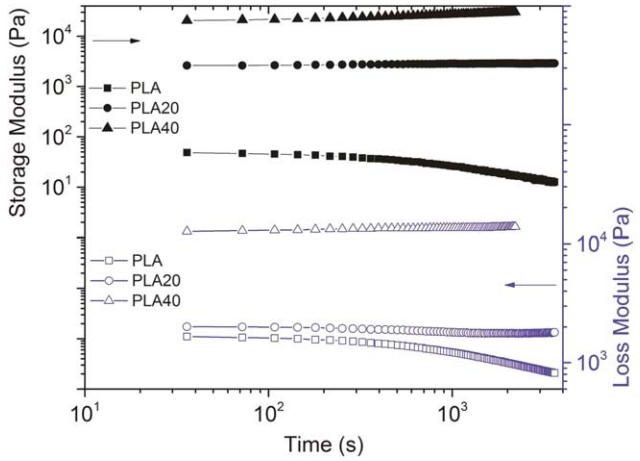

Figure 15. Stability of storage (filled symbols) and loss moduli (open symbols) during constant oscillation over time. [Color figure can be viewed in the online issue, which is available at wileyonlinelibrary.com.]

The —C═O stretching for pure TPU has a specific multiplet peak at ~1730 cm^{-1} due to being in urethane and ester groups, but —C═O stretching at ester groups in the PLA is a singlet at ~1751 cm^{-1}.[30] The blends show the carbonyl stretching peak at ester or urethane groups at lower wavenumbers (~1749 cm^{-1}) corresponding to the increased hydrogen bonding of —C═O, —OH, and —NH.[30,38,50] The main peaks in PLA5 are sharper than in PLA, but the peak heights of PLA25 are smaller than those of PLA. The discussed peak heights again had a rise in PLA40 compared to PLA25. These explanations mention that PLA25 has the lowest peak heights associated with better compatibility and dispersion of TPU in PLA. It is assumed that the enhanced interactions and hydrogen bonding in this sample broadened the peaks due to a larger TPU content (e.g., PLA40) in the blends. PLA and TPU have less interaction due to the different morphologies originating from the cocontinuity detracting from the interfacial surfaces between PLA and TPU. Actually, the TPU concentrations more than 25 wt % turn the morphology of the blend from sea-island to cocontinuous, so the most possible phase interactions occur in PLA25, which has the largest interfacial surfaces seen by the SEM.

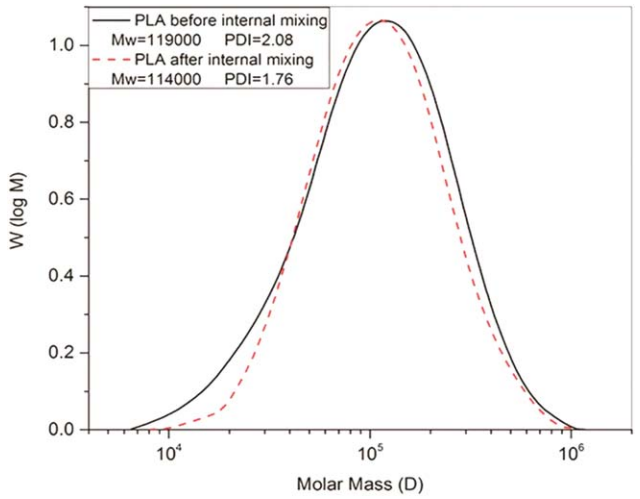

Figure 16. GPC curve and molecular weight of PLA before (solid line) and after (dashed line) internal mixing. [Color figure can be viewed in the online issue, which is available at wileyonlinelibrary.com.]

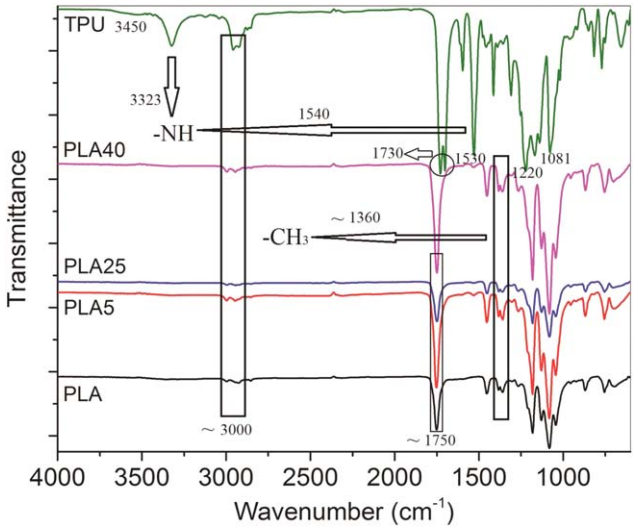

Figure 17. FTIR spectra of PLA, PLA5, PLA25, PLA40, and TPU. [Color figure can be viewed in the online issue, which is available at wileyonlinelibrary.com.]

CONCLUSIONS

In this study, PLA and TPU were melt-blended with an internal mixer, and the effect of the PLA/TPU ratio on the mechanical, thermal, rheological, chemical, and morphological properties of the blends was investigated. The toughness and mechanical strength of the sample coded PLA25 were improved while PLA was the dominating phase in the blend. The toughness of PLA25 was 4.3 times greater than that of the pure PLA. The PLA role as the dominating matrix in PLA25 led to a more biocompatible and biodegradable polymer blend. The DMTA results showed that, in PLA/TPU blends with TPU content lower than 30%, PLA is almost the predominant phase, showing only one T_g. The SEM showed the continuity of PLA in these blends and confirmed the DMTA results. The presence of a G′/G″ crossover point at low frequencies for the dynamic rheological response of the blends indicated the high viscoelasticity of the blends and high interactions between PLA and TPU. The FTIR characteristic peak heights of PLA25 were lower than those of the other samples, confirming compatibility. Also, the SEM phase images confirmed good compatibility of PLA25 due to the sea-island morphology leading to some large interfacial surfaces. Overall, this work presents a successful compatibilization method of PLA/TPU without compatibilizers but by using only ester-based TPU.

REFERENCES

1. Jamshidian, M.; Tehrany, E. A.; Imran, M.; Jacquot, M.; Desobry, S. *Compr. Rev. Food Sci. Food Saf.* **2010**, *9*, 552.

2. Xiao, L.; Wang, B.; Yang, G.; Gauthier, M. Biomedical Science, Engineering and Technology, Ghista D. (Ed.), ISBN: 978-953-307-471-9, InTech, 2012, http://www.intechopen.com/books/biomedical-science-engineering-and-technology/poly-lactic-acid-based-biomaterials-synthesis-modification-and-applications.
3. Vroman, I.; Tighzert, L. *Materials* **2009**, *2*, 307.
4. Barikani, M.; Oliaei, E.; Seddiqi, H.; Honarkar, H. *Iran. Polym. J.* **2014**, *23*, 307.
5. Davachi, S. M.; Kaffashi, B.; Roushandeh, J. M.; Torabinejad, B. *Mater. Sci. Eng. C* **2012**, *32*, 98.
6. Rasal, R. M.; Janorkar, A. V.; Hirt, D. E. *Prog. Polym. Sci.* **2010**, *35*, 338.
7. Garlotta, D. *J. Polym. Environ.* **2001**, *9*, 63.
8. Wang, S. C.; Xiang, H. X.; Wen, X. S.; Zhou, Z.; Zhu, M. F. *Mater. Sci. Forum* **2014**, *789*, 117.
9. Feng, F.; Zhao, X.; Ye, L. *J. Macromol. Sci. Phys.* **2011**, *50*, 1500.
10. Lai, S.; Lan, Y. *J. Polym. Res.* **2013**, *20*, 1.
11. Jing, X.; Mi, H. Y.; Peng, X. F.; Turng, L. S. *Polym. Eng. Sci.* **2015**, *55*, 70.
12. Wu, D.; Zhang, Y.; Zhang, M.; Zhou, W. *Eur. Polym. J.* **2008**, *44*, 2171.
13. Fu, Q.; Bai, H. W.; Xiu, H.; Huang, C. M. *Express Polym. Lett.* **2013**, *7*, 261.
14. Liu, H.; Yang, Y.; Shen, S.; Zhong, Z.; Zheng, L.; Feng, P. In Advances in Textile Engineering and Materials; Trans Tech Publications: Switzerland, **2013**; Chapter 1.
15. Jašo, V.; Cvetinov, M.; Rakić, S.; Petrović, Z. S. *J. Appl. Polym. Sci.* **2014**, *131*, 41104.
16. Kaynak, C.; Meyva, Y. *Polym. Adv. Tech.* **2014**, *25*, 1622.
17. Yu, R. l.; Zhang, L. S.; Feng, Y. H.; Zhang, R. Y.; Zhu, J. *Chin. J. Polym. Sci.* **2014**, *32*, 1099.
18. Liu, Z. W.; Chou, H. C.; Chen, S. H.; Tsao, C. T.; Chuang, C. N.; Cheng, L. C.; Yang, C. H.; Wang, C. K.; Hsieh, K. H. *Polym. Compos.* **2014**, *35*, 1744.
19. Davachi, S. M.; Kaffashi, B. *Polym. Plast. Tech. Eng.* **2015**, *54*, 944.
20. Peponi, L.; Navarro-Baena, I.; Sonseca, A.; Gimenez, E.; Marcos-Fernandez, A.; Kenny, J. M. *Eur. Polym. J.* **2013**, *49*, 893.
21. Mohammadi-Rovshandeh, J.; Pouresmaeel-Selakjani, P.; Davachi, S. M.; Kaffashi, B.; Hassani, A.; Bahmeyi, A. *J. Appl. Polym. Sci.* **2014**, *131*, 41095.
22. Han, J. J.; Huang, H. X. *J. Appl. Polym. Sci.* **2011**, *120*, 3217.
23. Yang, D. In Mechanical Engineering, Industrial Materials and Industrial Electronics; Trans Tech Publications: Switzerland, **2013**; Chapter 2.
24. Chen, Q.; Liang, S.; Thouas, G. A. *Prog. Polym. Sci.* **2013**, *38*, 584.
25. Hong, H.; Wei, J.; Yuan, Y.; Chen, F. P.; Wang, J.; Qu, X.; Liu, C. S. *J. Appl. Polym. Sci.* **2011**, *121*, 855.
26. Li, Y.; Shimizu, H. *Macromol. Biosci.* **2007**, *7*, 921.
27. Mi, H. Y.; Salick, M. R.; Jing, X.; Jacques, B. R.; Crone, W. C.; Peng, X. F.; Turng, L. S. *Mater. Sci. Eng. C* **2013**, *33*, 4767.
28. Yuan, Y.; Ruckenstein, E. *Polym. Bull.* **1998**, *40*, 485.
29. Feng, F.; Ye, L. *J. Appl. Polym. Sci.* **2011**, *119*, 2778.
30. Raja, M.; Ryu, S. H.; Shanmugharaj, A. M. *Eur. Polym. J.* **2013**, *49*, 3492.
31. Dogan, S. K.; Reyes, E. A.; Rastogi, S.; Ozkoc, G. *J. Appl. Polym. Sci.* **2014**, *131*, 40251.
32. Lim, L. T.; Auras, R.; Rubino, M. *Prog. Polymer Sci.* **2008**, *33*, 820.
33. Lederer, K.; Macko, T.; Imrich-Schwarz, G.; Aust, N.; Kolmanics, T.; Schwarz, T. *Appl. Macromol. Chem. Phys. Angew. Makromol. Chem.* **1996**, *241*, 113.
34. Imre, B.; Bedő, D.; Domján, A.; Schön, P.; Vancso, G. J.; Pukánszky, B. *Eur. Polym. J.* **2013**, *49*, 3104.
35. Riemenschneider, W.; Bolt, H. M. Esters, Organic. In Ullmann's Encyclopedia of Industrial Chemistry; Wiley-VCH: New York, **2005**.
36. Kaura, L.; Singh, J.; Singh, H.; McCarthy, O. J. *Food Chem.* **2008**, *111*, 1.
37. Ramkumar, D. H. S.; Bhattacharya, M. *Polym. Eng. Sci.* **1998**, *38*, 1426.
38. Davachi, S. M.; Kaffashi, B. *Int. J. Polym. Mater.* **2015**, *64*, 497.
39. Davachi, S. M.; Kaffashi, B.; Roushandeh, J. M. *Polym. Adv. Tech.* **2012**, *23*, 565.
40. Davachi, S. M.; Kaffashi, B.; Zamanian, A.; Torabinejad, B.; Ziaeirad, Z. *Mater. Sci. Eng. C Mater. Biol. Appl.* **2016**, *58*, 294.
41. Standard Test Method for Rubber Property-Abrasion Resistance (Rotary Drum Abrader); Designation: ASTM D 5963-97a, **2001**.
42. Kazakevi, R.; Özarmut, A. Ö.; Steeb, H. *Smart Mater. Res.* **2014**, *2014*, 1.
43. Oliaei, E.; Kaffashi, B.; Davachi, S. M. Presented at the 15th Iranian National Congress of Chemical Engineering, University of Tehran, Tehran, Iran, **2015**.
44. Poomali; Siddaramaiah; Suresha, B.; Lee, J. H. *Mater. Sci. Eng. A* **2008**, *492*, 486.
45. Torabinejad, B.; Mohammadi-Rovshande, J.; Davachi, S. M.; Zamanian, A. *Mater. Sci. Eng. C* **2014**, *42*, 199.
46. Mousavi, L.; Nazockdast, H.; Mohammadi, Y.; Azizi, H.; Saleh, Z. *J. Appl. Polym. Sci.* **2012**, *125*, E260.
47. Xiu, H.; Huang, C.; Bai, H.; Jiang, J.; Chen, F.; Deng, H.; Wang, K.; Zhang, Q.; Fu, Q. *Polymer* **2014**, *55*, 1593.
48. Cates, M. E.; Sollich, P. J. *Rheol.* **2004**, *48*, 193.
49. Sollich, P.; Lequeux, F.; Hébraud, P.; Cates, M. E. *Phys. Rev. Lett.* **1997**, *78*, 2020.
50. Wong, C. S.; Badri, K. H. *Mater. Sci. Appl.* **2012**, *3*, 78.